Indian J Phys (March 2022) 96(4):1193–1203
https://doi.org/10.1007/s12648-021-02065-6

ORIGINAL PAPER

A conservative numerical scheme for capturing interactions of optical solitons in a 2D coupled nonlinear Schrödinger system

M M Mousa[1,2]* and W-X Ma[3,4,5,6]*

[1]Department of Basic Sciences, Faculty of Engineering at Benha, Benha University, Benha 13512, Egypt

[2]Department of Mathematics, College of Sciences and Human Studies at Hotat Sudair, Majmaah University, Majmaah 11952, Saudi Arabia

[3]Department of Mathematics and Statistics, University of South Florida, Tampa, FL 33620, USA

[4]Department of Mathematics, Zhejiang Normal University, Jinhua 321004, Zhejiang, China

[5]Department of Mathematics, King Abdulaziz University, Jeddah 21589, Saudi Arabia

[6]School of Mathematical and Statistical Sciences, North-West University, Mafikeng Campus, Private Bag X2046, Mmabatho 2735, South Africa

Received: 15 September 2020 / Accepted: 23 February 2021 / Published online: 25 March 2021

Abstract: In this study, an efficient fourth-order conservative explicit numerical scheme using method of lines is developed to simulate different scenarios of soliton interactions and reflections for a (2 + 1)-dimensional coupled nonlinear Schrödinger (CNLS) system. The fourth-order Runge–Kutta technique is applied as a time integrator to the resulting ordinary differential system. Both integrable and nonintegrable cases of the CNLS system are considered. A condition for the scheme to be stable is deduced with the aid of von Neumann stability analysis. Several numerical experiments have been carried out to exhibit the reliability of the scheme in capturing and understanding the interesting phenomenon of elastic and inelastic soliton collisions/reflections related to many nonlinear evolution equations. The ability of the scheme to preserve the conserved invariants in long terms confirms its accuracy and stability. New results associated with interactions and reflections of soliton waves are obtained.

Keywords: Coupled nonlinear Schrödinger equation; Method of lines; Soliton interactions; Soliton reflections

1. Introduction

Various forms of nonlinear Schrödinger equations are used in several applications, such as Bose–Einstein condensates of atoms, plasma physics, systems of fiber communications, nonlinear optics, quantum mechanics and fluid dynamics [1–9]. Concerning the field of communication in fiber systems, such systems have been exposed to describe spread of waves in nonlinear optical fibers and in the systems of wavelength-division-multiplexed [2, 10]. Also, the beam propagation in crystals is modeled using this type of equations. In [5], the propagation of interaction solitons is imaged at real time and discovered using the atoms condensates of Bose–Einstein with awesome collisions by a quasi-one-dimensional waveguide. Also, the spread of rogue waves in open water is described by the nonlinear Schrödinger equation [11]. Solitary waves produced by the coupled nonlinear Schrödinger (CNLS) equations are often termed by vector solitons as they naturally have two components. In the last recent years, the (1 + 1)-dimensional CNLS system has been numerically examined intensively [12–14]. It is proven that the vector soliton can pass through each other after the collision and can be bounced off or trapped each other depending on the collision type. But there is a lack of investigations that have numerically examined the soliton collisions/reflections for (2 + 1)-dimensional CNLS systems [15–17]. From the previous discussion, the study of the soliton interactions (collisions/reflections) for (2 + 1)-dimensional CNLS systems is a significant issue.

In this study, we consider a (2 + 1)-dimensional system of coupled nonlinear Schrödinger equation in a general form [16]:

*Corresponding author, E-mail: mm.mousa@mu.edu.sa; mawx@cas.usf.edu

$$\begin{cases} \mathrm{i}U_t + \gamma(U_{xx} + U_{yy}) + \alpha\left(|U|^2 + \beta|V|^2\right)U = 0, \\ \mathrm{i}V_t + \gamma(V_{xx} + V_{yy}) + \alpha\left(\beta|U|^2 + |V|^2\right)V = 0, & \text{in } \Omega \times [0, T], \\ U(x, y, 0) = U_0,\ V(x, y, 0) = V_0, & \text{in } \Omega. \end{cases} \tag{1}$$

The solution of (1) has the following conservation invariants,

$$\begin{aligned} Q_1(t) &= \int_{-\infty}^{\infty}\int_{-\infty}^{\infty} |U|^2 \mathrm{d}x\mathrm{d}y, Q_2(t) = \int_{-\infty}^{\infty}\int_{-\infty}^{\infty} |V|^2 \mathrm{d}x\mathrm{d}y, \\ Q_3(t) &= \int_{-\infty}^{\infty}\int_{-\infty}^{\infty} \gamma\left(|U_x|^2 + |U_y|^2 + |V_x|^2 + |V_y|^2\right) \\ &\quad - \frac{\alpha}{2}\left(|U|^4 + |V|^4\right) - \beta\,|U|^2|V|^2 \mathrm{d}x\mathrm{d}y, \end{aligned} \tag{2}$$

where Q_1 and Q_2 are called the mass conservation while Q_3 is called the energy conservation. These invariants satisfy the conditions: $\mathrm{d}Q_1/\mathrm{d}t = \mathrm{d}Q_2/\mathrm{d}t = \mathrm{d}Q_3/\mathrm{d}t = 0$. Here, $\Omega \in \mathbb{R}^2$ is a bounded domain, $\mathrm{T} < \infty$ and $\mathrm{i} = \sqrt{-1}$, where the functions U, V are complex functions in x, y and t, that represent the solutions of system (1). In nonlinear optics, it is commonly termed that $|U|^2$ and $|V|^2$ represent the optical power while the parameters α, β and γ represent Landau constant, wave–wave collision coefficient (coupling coefficient) and dispersion coefficient, respectively. These parameters are considered real and their values differ for various polarizations in nonlinear optics or for different types of geophysical fluid flows. When $\beta = 0$, the CNLS system (1) turns into 2 decoupled nonlinear Schrödinger (NLS) equations, whereas for $\beta = 1$, the considered system is transformed into Manakov system. Both the decoupled NLS system and Manakov system are integrable and the interaction of their soliton waves shows the elastic collision. However, for other values of β, The CNLS system becomes nonintegrable where the solitons interaction is called inelastic collision. In this case, many complex phenomena such as transmission of solitons, reflection of solitons, fusion of solitons and creation of a new vector soliton can occur. It is known that for (1 + 1)-dimensional integrable systems of coupled nonlinear Schrödinger equations, one can analytically only find exact solutions describing soliton reflections. However, in the (2 + 1)-dimensional case, these systems loss their integrability and hence we have to utilize numerical methods for discovering the phenomena of soliton–wall reflection and soliton–soliton collision. In the literature, there are limited studies that investigate analytically the soliton interactions and reflections for (1 + 1)-dimensional integrable systems [18–21]. Various numerical techniques have been utilized for solving many nonlinear Schrödinger-type equations [22–25]. Recently, the soliton reflections from different rigid walls for the (2 + 1)-dimensional cubic NLS equations are numerically simulated using a Crank–Nicolson finite element technique [26], in which the authors examined the reflection of a single solitary wave for a nonlinear Schrödinger equation subjected to three different boundary conditions. In our study, we extend the study of [26] to simulate both of reflections and collisions soliton waves for 2D coupled nonlinear Schrödinger system using a forth order robust numerical scheme based on the well-known method of lines (MOL) [27–31]. The proposed numerical scheme is inspected for stability and accurateness. The developed scheme is conditionally stable in its linearized form based on von Neumann stability analysis. The scenarios of soliton–soliton and soliton–wall interactions need that the considered system is subjected to pre-defined boundary conditions. Both zero-Dirichlet and zero-Neumann boundary conditions are considered in the current work.

This paper is prepared as follows: in the next section, we briefly clarify the MOL and construct a fourth-order explicit numerical scheme for the (2 + 1)-dimensional CNLS system. Section 3 contains the stability condition based on linearized von Neumann stability. Several numerical tests with different initial data are considered in Sect. 4. Simulation of many scenarios that describe elastic and inelastic soliton waves reflections and collisions for the (2 + 1)-dimensional CNLS system are also illustrated in Sect. 4. Conclusions are composed in Sect. 5.

2. Numerical scheme

In order to use the MOL for solving system (1), we must decompose the dependent variables U, V in their real and imaginary parts using,

$$\begin{cases} U = P_1 + \mathrm{i}P_2 \\ V = P_3 + \mathrm{i}P_4 \end{cases}, \tag{3}$$

where $\{P_j\}_{j=1}^4$ are real-valued functions. By substituting Eq. (3) into system (1), we can obtain the following matrix form system:

$$\mathbf{P}_t + \gamma\mathbf{A}\left(\mathbf{P}_{xx} + \mathbf{P}_{yy}\right) + \alpha\mathbf{F}(\mathbf{P})\mathbf{P} = \mathbf{0}, \tag{4}$$

where

$$\mathbf{P} = \begin{bmatrix} P_1 \\ P_2 \\ P_3 \\ P_4 \end{bmatrix}, \mathbf{A} = \begin{bmatrix} 0 & 1 & 0 & 0 \\ -1 & 0 & 0 & 0 \\ 0 & 0 & 0 & 1 \\ 0 & 0 & -1 & 0 \end{bmatrix}, \mathbf{F}(\mathbf{P}) = \begin{bmatrix} 0 & q_1 & 0 & 0 \\ -q_1 & 0 & 0 & 0 \\ 0 & 0 & 0 & q_2 \\ 0 & 0 & -q_2 & 0 \end{bmatrix},$$

$q_1 = \left(P_1^2 + P_2^2\right) + \beta\left(P_3^2 + P_4^2\right)$ and $q_2 = \beta\left(P_1^2 + P_2^2\right) + \left(P_3^2 + P_4^2\right)$.

Now, the spatial coordinates x and y in system (4) will be discretized with a uniformly rectangular mesh of $M \times N$ points, where $x_l = a + l\ h$, $y_m = b + m\ k$, $l = 1, 2,..., M$, $m = 1, 2,..., N$, $\Omega = [a, b] \times [c, d]$ and $h = (b - a)/M$, $k = (d - c)/N$ are the spatial step sizes of the grid. A fourth-order central finite difference formula is used to approximate the spatial second-degree derivatives at each mesh point. Then, the fourth-order Runge–Kutta method (RK4) is applied as time integrator for solving the resulting first-order ordinary differential equations subjected to the pre-defined initial data using a suitable time step τ in the range $0 \le t \le T$. Applying a fourth-order central difference operator to system (4) gives the following first-order ordinary differential equations system,

$$\frac{\mathrm{d}\mathbf{P}_{l,m}}{\mathrm{d}t} = \mathbf{S}\left(\mathbf{P}_{l,m}\right), \tag{5}$$

where

$$\mathbf{S}\left(\mathbf{P}_{l,m}\right) = \frac{\gamma}{12}\mathbf{A}\begin{pmatrix} \frac{1}{h^2}\left(\mathbf{P}_{l-2,m} - 16\mathbf{P}_{l-1,m} + 30\mathbf{P}_{l,m} - 16\mathbf{P}_{l+1,m} + \mathbf{P}_{l+2,m}\right) \\ +\frac{1}{k^2}\left(\mathbf{P}_{l,m-2} - 16\mathbf{P}_{l,m-1} + 30\mathbf{P}_{l,m} - 16\mathbf{P}_{l,m+1} + \mathbf{P}_{l,m+2}\right) \end{pmatrix} - \alpha\mathbf{F}\left(\mathbf{P}_{l,m}\right)\mathbf{P}_{l,m}. \tag{6}$$

Using the RK4, the solution of system (5) will be calculated as follows:

$$\mathbf{P}_{l,m}^{n+1} = \mathbf{P}_{l,m}^{n} + \frac{1}{6}\left[\mathbf{L_1} + 2\mathbf{L_2} + 2\mathbf{L}_3 + \mathbf{L_4}\right], \tag{7}$$

where n is the time index and

$$\mathbf{L_1} = \tau\,\mathbf{S}\left(\mathbf{P}_{l,m}^{n}\right),\ \mathbf{L_2} = \tau\,\mathbf{S}\left(\mathbf{P}_{l,m}^{n} + \frac{1}{2}\mathbf{L_1}\right),$$
$$\mathbf{L_3} = \tau\,\mathbf{S}\left(\mathbf{P}_{l,m}^{n} + \frac{1}{2}\mathbf{L_2}\right),\ \mathbf{L_4} = \tau\,\mathbf{S}\left(\mathbf{P}_{l,m}^{n} + \mathbf{L_3}\right). \tag{8}$$

The explicit finite difference scheme (7) is of 4th order in both time and space. It is easy to apply, and it is predicted to give accurate results as we will discuss later. The only disadvantage of the scheme is stability restriction that will be discussed in the succeeding section.

3. Stability restriction

To deduce the stability condition for the finite difference scheme (7), we use a linearized von Neumann stability analysis [32]. The linear version of system (4) can be written as follows:

$$\mathbf{P}_t = -\gamma\mathbf{A}\left(\mathbf{P}_{xx} + \mathbf{P}_{yy}\right) - \alpha\, q\,\mathbf{A}\,\mathbf{P}, \tag{9}$$

where $q = \max\{q_1, q_2\}$.

Based on the von Neumann stability method, one can write the solution of the linearized system (9) in single Fourier mode as

$$\mathbf{P}_{l,m}^{n} = \xi^n\, e^{\mathrm{i}\lambda l h}\, e^{\mathrm{i}\delta m k},\ l = 1, 2, \ldots, M \text{ and } m = 1, 2, \ldots, N, \tag{10}$$

where ξ is the amplification vector and the parameters λ, δ are real constants. Substitution (10) in system (9) gives to the following equation,

$$\widetilde{\mathbf{S}}\left(\mathbf{P}_{l,m}^{n}\right) = \varepsilon\,\mathbf{A}\,\mathbf{P}_{l,m}^{n}. \tag{11}$$

where $\widetilde{\mathbf{S}}$ is the RHS of system (9) after spatial derivatives discretization and the parameter ε is defined as

$$\varepsilon = \frac{\gamma}{12}\left[\frac{1}{h^2}\left(2\cos(2\lambda h) - 32\cos(\lambda h) + 30\right) + \frac{1}{k^2}\left(2\cos(2\delta k) - 32\cos(\delta k) + 30\right)\right] - \alpha\, q. \tag{12}$$

Substituting of (11) into (7) gives to the following matrix form equation:

$$\mathbf{B} = \mathbf{I} + \sum_{j=1}^{4}\frac{1}{j!}\left(\tau\,\varepsilon\,\mathbf{A}\right)^j, \tag{13}$$

where $\mathbf{I}$ means the identity matrix. The eigenvalues of the matrix $\mathbf{B}$ are notated by $\aleph$. Based on to the von Neumann analysis, the required condition needed for the scheme stability is that $\max_j\left|\aleph_j\right| \le 1$, $j = 1, 2, ..., 4$. Computing for the matrix $\mathbf{B}$ eigenvalues, we get

$$\left|\aleph_j\right|^2 = 1 - \frac{(\tau\,\varepsilon)^6}{72} + \frac{(\tau\,\varepsilon)^8}{576},\ \forall j = 1, 2, ..., 4. \tag{14}$$

From Eqs. (12) and (14), we can guarantee that $\left|\aleph_j\right| \le 1$ if the following condition is satisfied,

$$\tau \le \frac{3\sqrt{2}}{16\gamma\left[(h^2)^{-1} + (k^2)^{-1}\right] - 3\,\alpha\, q}. \tag{15}$$

4. Numerical tests

To examine the effectives of the scheme in simulating soliton interactions for the (2 + 1)-dimensional CNLS system, we consider several numerical examples related to system (1). The conservation of the scheme is inspected by computing the mass and energy conserved quantities at different times. We use the composite trapezoidal rule to calculate the integrals associated with the conserved quantities. Zero-Neumann boundary conditions ($\partial U/\partial n = \partial V/\partial n = 0$, on $\partial\Omega$) are applied to all boundaries of the considered numerical tests. As a generalization to all

numerical tests, we also solved the first test subjected to zero-Dirichlet boundary conditions ($U = V = 0$, on $\partial\Omega$) to illustrate how the solitons interact to the boundary for both boundary conditions types. For all considered numerical examples, the solutions are calculated for the following parameters $\gamma = 1/2$, $\alpha = 1$, to study the impact of the wave–wave collision coefficient β on the interactions of the vector soliton. The step sizes of space and time are selected as $h = 0.05$, $k = 0.02$ and $\tau = 10^{-4}$, over the domain $\Omega = [-20, 20] \times [-5, 5]$ up to time $T = 60$.

4.1. Elastic interaction of three superposition solitons

Firstly, we consider system (1) subjected to the initial conditions defined by a superposition of three soliton waves that propagate with different velocities with dissimilar initial locations and amplitudes. Here, we use the following initial conditions considered in [12],

$$U_0 = V_0 = \sum_{m=1}^{3} \sqrt{\frac{2\eta_m}{\beta+1}} \operatorname{sech}\left(\sqrt{2\eta_m}\,(x - x_m)\right) e^{i(s_m(x-x_m))}, \tag{16}$$

where x_m, s_m and η_m are arbitrary parameters standing for soliton wave initial locations, velocities and widths/amplitudes, respectively. Here, the parameters are selected as follows: $\eta_1 = 1.0$, $\eta_2 = 0.5$, $\eta_3 = 0.8$, $s_1 = 1.0$, $s_2 = 0.1$, $s_3 = -1.0$, $x_1 = -10$, $x_2 = 0$, $x_3 = 10$ and $\beta = 2/3$. Here, the profiles of the solutions U and V are identical. The solutions are obtained in the case of Neumann and Dirichlet boundary conditions to display in what way the soliton interaction to the boundaries becomes in each case. The modulus value of the solutions $|U|$ and $|V|$ are plotted for selected values of t. The trajectories of the interactions and reflections of the three solitons for selected moments are displayed in Fig. 1.

For more clarification of soliton interactions, contours and 3D surface illustrations that describe the profiles of $|U|$ and $|V|$ along the horizontal cross section line ($y = 0$) are displayed in Fig. 2 (when using zero-Neumann boundary conditions) and Fig. 3 (when using zero-Dirichlet boundary conditions) up to $t = 60$. From the interaction scenario of the three solitons displayed in Figs. 1, 2 and 3, one can see that two of them propagate in the same direction with unlike speeds, while the third soliton moves in the opposite direction before reflecting two of them from the wall. After the solitons–wall reflection, the reflected waves reverse their directions. The solitons–wall interaction is perfect (elastic) for both the Dirichlet and Neumann boundary conditions, however the soliton shapes at the boundaries are slightly different. It is worth noting that the solitons elastically collided each other and departure the collision region unchanged in speeds or shapes. During the simulation period, there are two soliton–wall reflections of the fast waves that initially positioned at $x = -10$ and $x = 10$, near $t \approx 28.5$. The reflected waves experience a slight deformation in their shapes after the collision with the walls and then retain their initial shapes when reversing their directions. Here, the solitons can experience an unlimited number of interactions without any decaying in their energy during the propagation because of the nature of the elastic interaction.

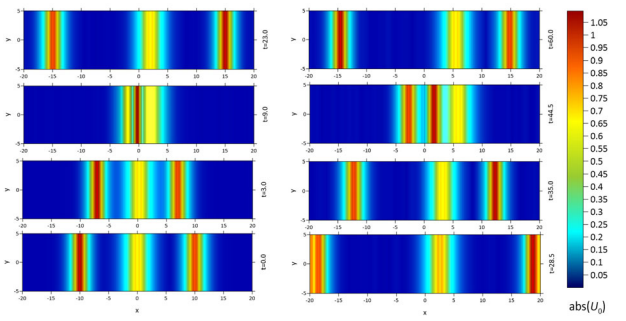

Fig. 1 Trajectory of three solitons elastic interactions at selected moments

In Table 1, the mass and energy conserved quantities Q_1, Q_2 and Q_3 at selected moments are listed in the case of using zero-Neumann boundary conditions. The values of the conserved invariants at $t = 0$ are estimated by integrating (2) numerically when $U = U_0$ and $V = V_0$ over the considered domain Ω. From Table 1, it can be observed that the mass quantities Q_1 and Q_2 are exactly conserved at 44.1501696 while the energy quantity Q_3 is almost conserved at 8.683.

4.2. Inelastic interactions of two different solitons

In the next numerical experiments, we consider five interaction scenarios that describe the inelastic vector soliton interactions. Some of such scenarios are informed in [8, 12] for (1 + 1)-dimensional NLS systems. The inelastic interactions occur when the coupled nonlinear Schrödinger system isn't integrable. The value of the coupling coefficient β plays a significant role in shaping the behavior of vector soliton interaction in a long-term simulation. Here, system (1) is solved corresponding to zero-Neumann boundary conditions and the next initial soliton waves,

$$\begin{aligned} U_0 &= \sqrt{2\eta_1}\operatorname{sech}\left(\sqrt{2\eta_1}\,(x - x_1)\right) e^{i(s_1 x)}, \\ V_0 &= \sqrt{2\eta_2}\operatorname{sech}\left(\sqrt{2\eta_2}\,(x - x_2)\right) e^{i(s_2 x)}. \end{aligned} \tag{17}$$

Here, the two initial solitons are selected in such a way that they move in an opposite direction with equal velocity,

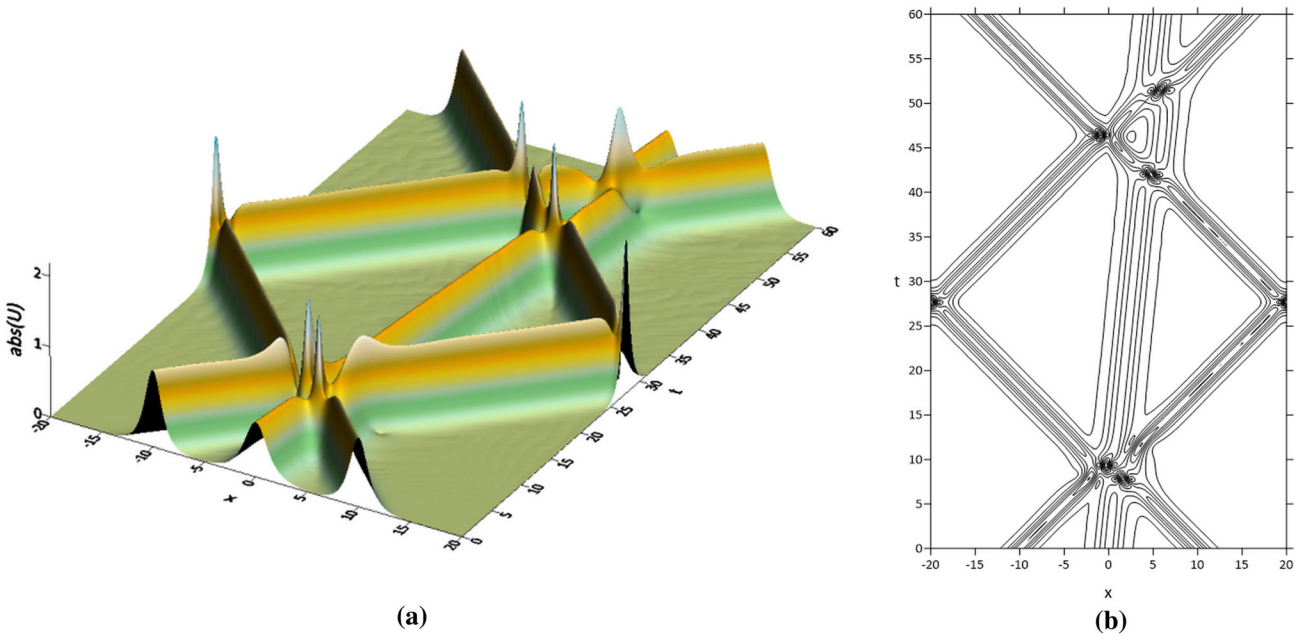

Fig. 2 (**a**) 3D surface plot and (**b**) contour plot of $|U|$ and $|V|$ along the line $y = 0$ in case of three solitons interactions (when applying zero-Neumann conditions)

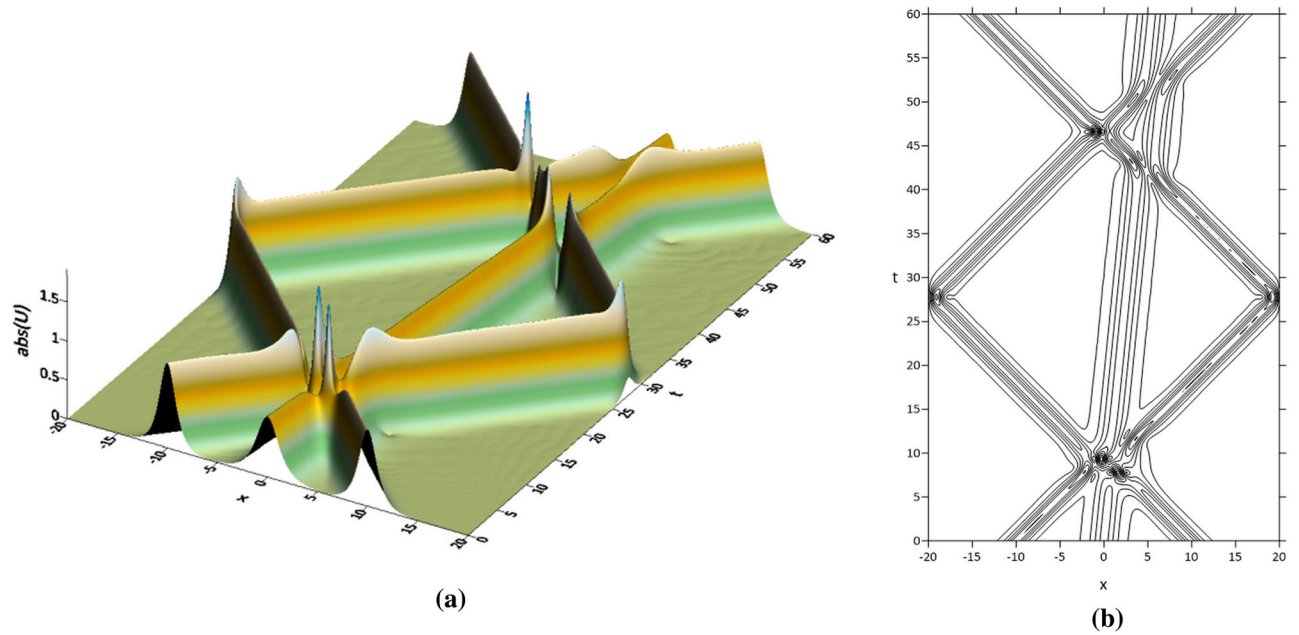

Fig. 3 (**a**) 3D surface plot and (**b**) contour plot of $|U|$ and $|V|$ along the line $y = 0$ in case of three solitons interactions (when applying zero-Dirichlet conditions)

dissimilar initial locations and different amplitudes. For all considered tests, we fix parameters of wave initial positions and wave widths/amplitudes as $x_1 = -10$, $x_2 = 10$, $\eta_1 = 1.1$ and $\eta_2 = 1.0$.

4.2.1. Scenario 1 (Soliton transmission)

Firstly, we select $\beta = 0.6$ and $s_1 = -s_2 = 0.8$. In this case, the value of β is moderate and the velocity of the waves is relatively high. The scenario of soliton–soliton collisions and solitons–walls reflections is shown in Figs. 4 and 5. As shown in these figures, the two waves collided around at

Table 1 Mass and energy conserved quantities of numerical test 4.1 at selected moments

t	Q_1, Q_2	Q_3	t	Q_1, Q_2	Q_3
0.0	44.15016965	8.682933350	28.5	44.15016962	8.682813740
3.0	44.15016966	8.682933350	35.0	44.15016962	8.682933865
9.0	44.15016966	8.682933295	44.5	44.15016964	8.682933370
23.0	44.15016965	8.682933980	60.0	44.15016960	8.682934780

$t \approx 13$. After the soliton collision, the two waves pass through each other with a slight variation in their profiles and daughter waves are transmitted with some radiation shedding (small wavelets). The generated daughter waves are small waves that split off from the original wave and spread alongside it but in a reversed direction. The amplitudes of the daughter pulses and the quantity of the generated wavelets are dependent on the value of β and on the initial soliton's velocities. Both original solitons and daughter waves hit the boundaries and reflected at the same time, approximately at $t \approx 37$. This means that the velocities of the waves remain equal after the soliton collision. The soliton and daughter waves experience some changing in their shapes during the reflection moment and then retrieve their initial shapes but in a reverse direction with little energy decaying. Up to $t = 60$, the mass quantities Q_1 and Q_2 are exactly conserved at 29.664794 and 28.284271, respectively, while the energy quantity Q_3 is conserved at $-$ 1.8859 for all moments excluding the values calculated during the moment of waves–walls reflections, e.g., $Q_3(37) = -$ 1.7901. After the reflection, Q_3 retrieves its conservative value of $-$ 1.8859 until the end of the simulation.

4.2.2. *Scenario 2 (Soliton reflection)*

In this numerical test, we select $\beta = -$ 0.6 and $s_1 = -s_2 = 0.8$. Here, we change the sign of the parameter β to investigate soliton interactions when $\beta < 0$. This scenario is displayed in Figs. 6 and 7. In this case, when sign of β is negative, the two originally soliton waves don't pass through each other but break up and reflected off each other after the collision (around at $t \approx 13$). For each wave, the large part of the energy is reflected while the remaining portion is transmitted causing some radiations shedding and wavelets. The amount of the developed radiations depends on the value of the relative speed $s_1 - s_2$. It can be realized that after the soliton–soliton reflection, each wave travels in an opposite direction until the collision to the walls and hence recovers its initial direction. The left wave is reflected once again from the left wall at $t \approx 41.2$ while the right wave is reflected from the right wall at $t \approx 38.2$. This difference in the time at which the two waves hit the boundaries is due to the different velocities after their collision. The left wave obviously gains some energy from the right one during the collision. Throughout the period of the simulation, the conserved invariants Q_1, Q_2 and Q_3 are precisely conserved at the same values of scenario 1 except the invariant Q_3 at the moments in which the waves hit and reflect from the walls. For example, and not as a limitation, $Q_3(38.2) = -$ 2.4274 and $Q_3(41.2) = -$ 1.0643. After the wave–wall reflection, Q_3 recovers its quantity of – 1.8859 until the end of the simulation. If the relative speed is large, then the two solitons pass through each other as shown in Fig. 8 which presents the interaction when $s_1 = -s_2 = 2$ (large relative speed) and $\beta = -$ 0.6.

4.2.3. *Scenario 3 (creation of new transmission vector soliton)*

In this scenario, we simulate a formation of new transmission vector soliton when the coupling coefficient β takes a large positive value with a small relative speed. Here, we chose $\beta = 3$ and $s_1 = -s_2 = 0.4$. The profile of the interactions of the vector soliton is displayed in Figs. 9 and 10. As illustrated in these figures, the interactions expose new structures. After collision (around at $t \approx 24$), the two soliton waves are meaningfully reshaped, bulky daughter waves are formed and radiations are shed as well. The new waves that are generated after the collision travel at velocities and directions very different from those of the initial two soliton waves. Commonly, large positive values of β, the interactions become quantitatively complex but qualitatively simple. After collision, the outcome is a few stable standing waves collected with some small wavelets and radiations. Up to $t = 60$, Q_1 and Q_2 are accurately conserved at 29.664794 and 28.284271, respectively, while Q_3 is almost conserved at $-$ 15.7359 for all moments excluding the values calculated during the moment of waves–walls interaction, e.g., $Q_3(41) = -$ 15.2304 and $Q_3(43.5) = -$ 16.9449.

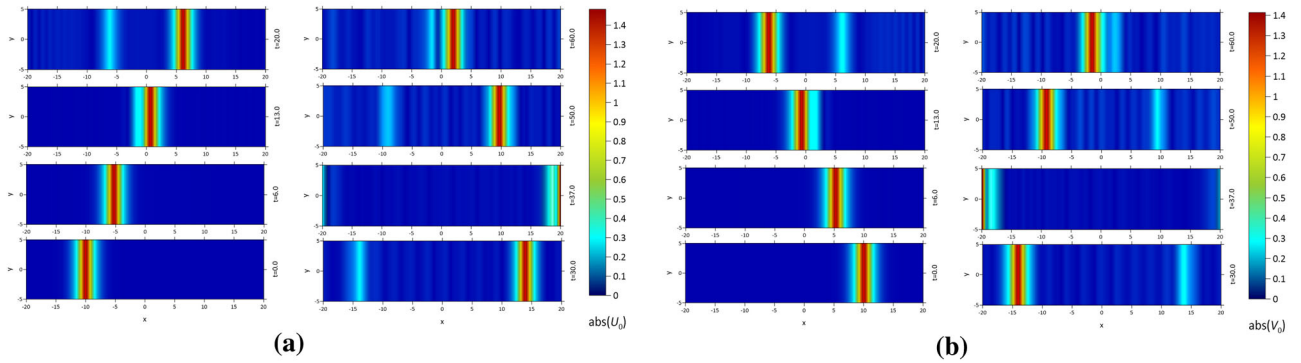

Fig. 4 Trajectory of scenario 1 interactions when $\beta = 0.6$ and $s_1 = -s_2 = 0.8$, (a) $|U|$ and (**b**) $|V|$

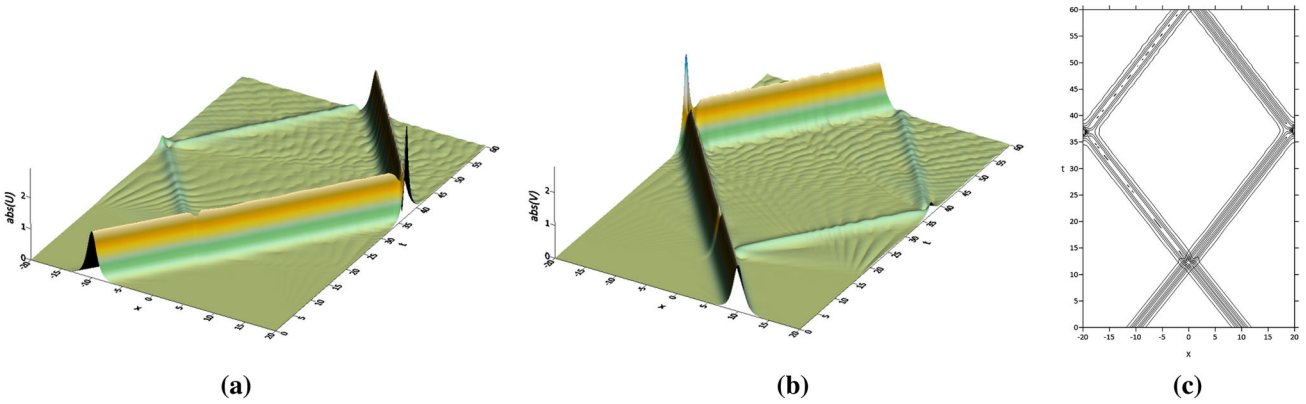

Fig. 5 (**a**) 3D surface plot of $|U|$, (**b**) 3D surface plot of $|V|$ and (c) contours plot of $|U|$ and $|V|$ together along the line $y = 0$ when $\beta = 0.6$ and $s_1 = -s_2 = 0.8$

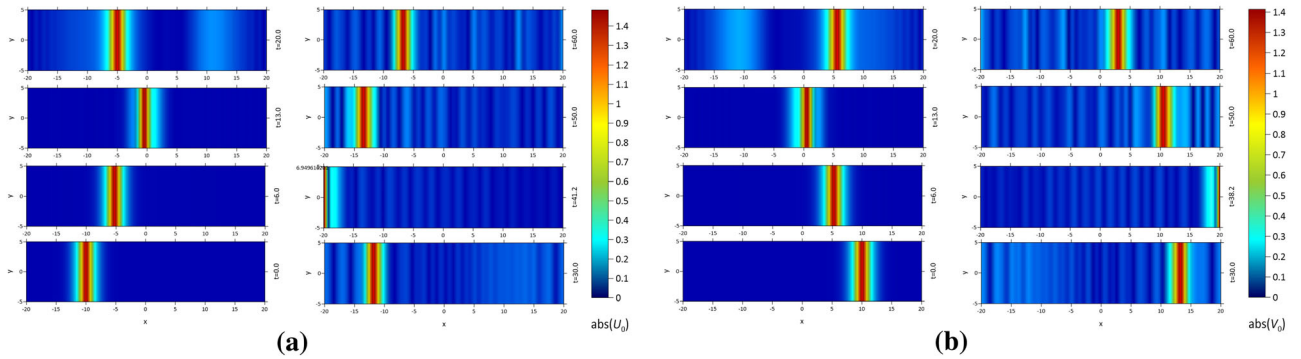

Fig. 6 Trajectory of scenario 2 interactions when $\beta = -0.6$ and $s_1 = -s_2 = 0.8$, (**a**) $|U|$ and (**b**) $|V|$

4.2.4. Scenario 4 (Creation of new reflection vector soliton)

In this scenario, we consider $s_1 = -s_2 = 0.4$ and $\beta = -3$. The behavior of the interaction of this vector soliton is presented in Figs. 11 and 12. It can be shown that after the soliton collision (around at $t \approx 24$), each wave is totally reflected and traveled in an opposite direction. This occurs when selecting a small relative speed with a large negative value of the coupling coefficient β. Here, the transmitted wavelets and radiations are almost negligible because the relative speed is small. During the computational time, the waves don't interact with the wall because of considering a slow wave velocity. The mass and energy invariants Q_1, Q_2 and Q_3 are precisely conserved at 29.664794, 28.284271 and -15.735882, respectively, up to $t = 60$.

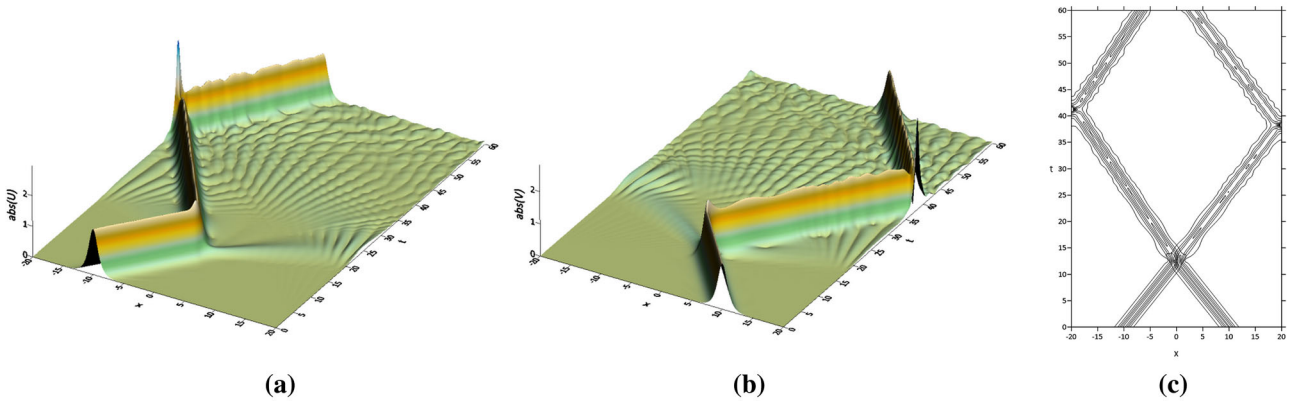

Fig. 7 (**a**) 3D surface plot of $|U|$, (**b**) 3D surface plot of $|V|$ and (**c**) contours plot of $|U|$ and $|V|$ together along the line $y = 0$ when $\beta = -0.6$ and $s_1 = -s_2 = 0.8$

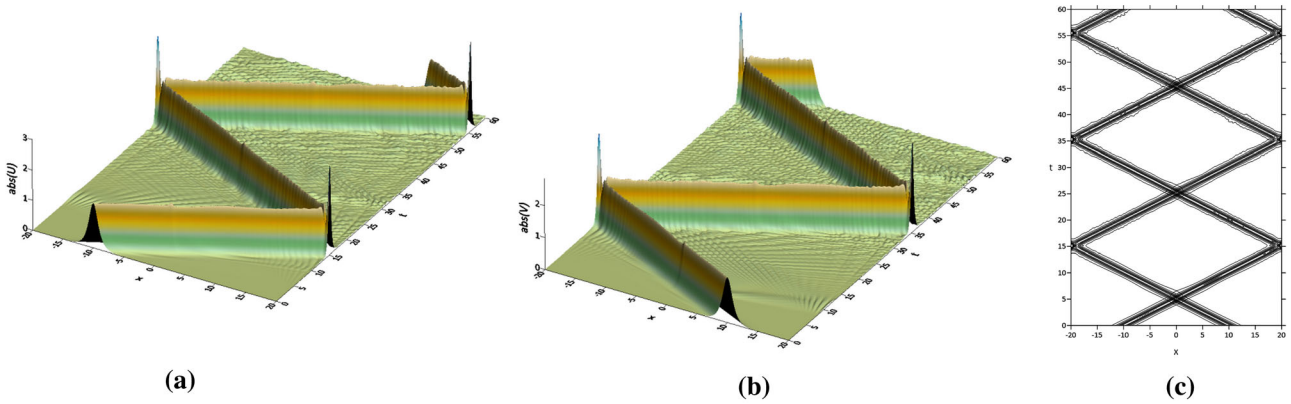

Fig. 8 (**a**) 3D surface plot of $|U|$, (**b**) 3D surface plot of $|V|$ and (**c**) contours plot of $|U|$ and $|V|$ together along the line $y = 0$ when $\beta = -0.6$ and $s_1 = -s_2 = 2$

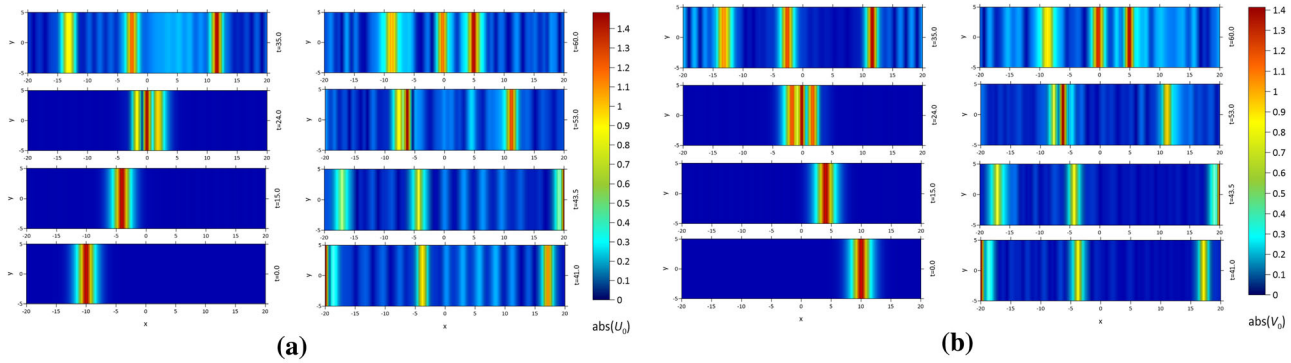

Fig. 9 Trajectory of scenario 3 interactions when $\beta = 3$ and $s_1 = -s_2 = 0.4$, (**a**) $|U|$ and (**b**) $|V|$

4.2.5. Scenario 5 (Soliton fusion)

Finally, we consider a small positive value coupling coefficient and a small relative speed. The parameters are chosen as $\beta = 0.2$ and $s_1 = -s_2 = 0.3$. The profile of this scenario is illustrated in Figs. 13 and 14. It can be noticed that the two soliton waves fusion into one wave after the collision occurs around at $t \approx 33$. The fusion of two solitons commonly occurs when selecting small positive value β and small value of the relative speed. Concerning the conserved quantities, Q_1, Q_2 and Q_3 are exactly conserved at 29.664794, 28.284271 and $-$ 17.7566, respectively, throughout the simulation period.

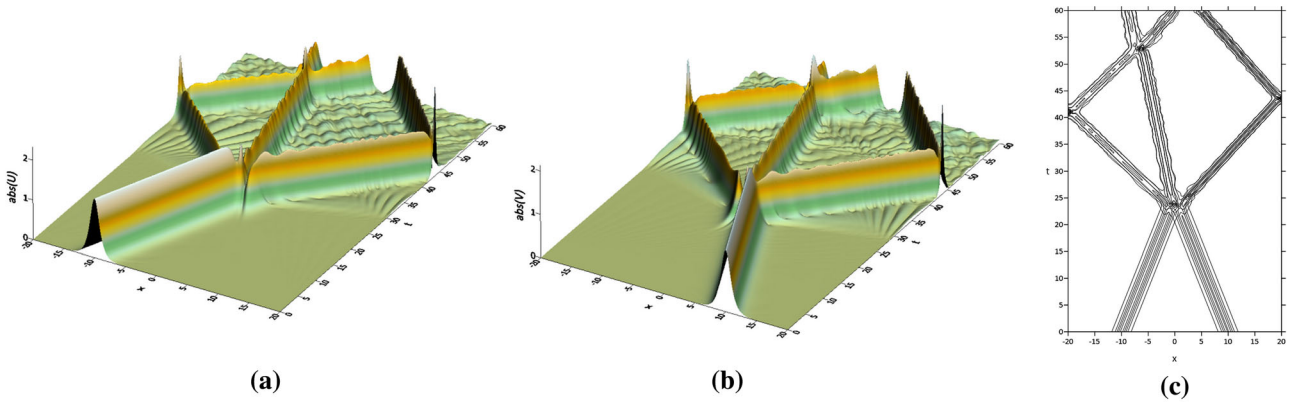

Fig. 10 (**a**) 3D surface plot of $|U|$, (**b**) 3D surface plot of $|V|$ and (c) contours plot of $|U|$ and $|V|$ together along the line $y = 0$ when $\beta = 3$ and $s_1 = -s_2 = 0.4$

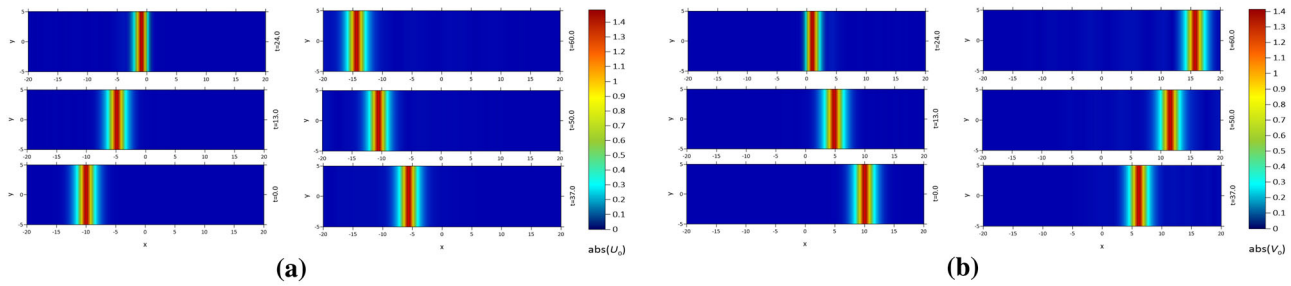

Fig. 11 Trajectory of scenario 4 interactions when $\beta = -3$ and $s_1 = -s_2 = 0.4$, (**a**) $|U|$ and (**b**) $|V|$

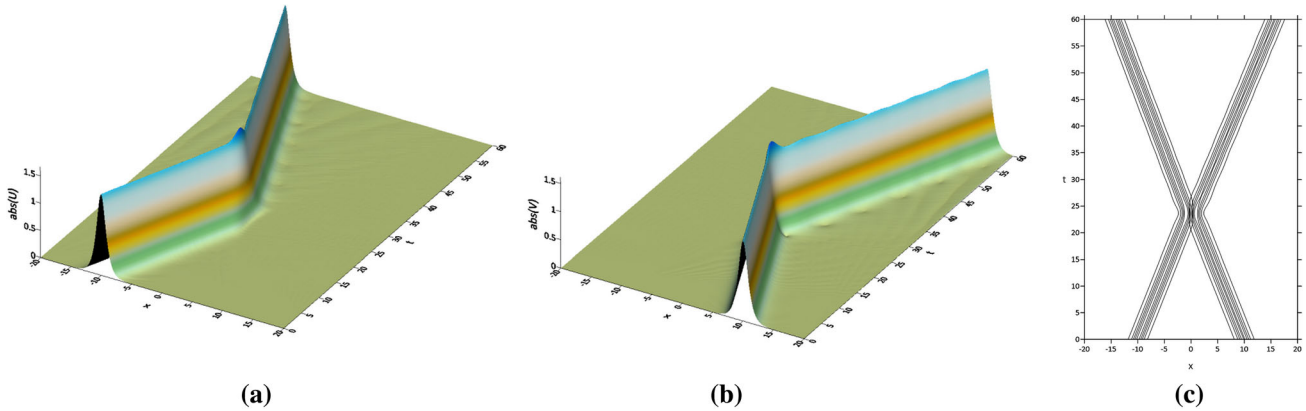

Fig. 12 (**a**) 3D surface plot of $|U|$, (**b**) 3D surface plot of $|V|$ and (c) contours plot of $|U|$ and $|V|$ together along the line $y = 0$ when $\beta = -3$ and $s_1 = -s_2 = 0.4$

5. Conclusions

In this work, a robust fourth-order conservative numerical scheme was developed and analyzed to capture different types of soliton interactions and reflection scenario for 2D CNLS system. The stability restriction of the scheme was deduced. The ability of the scheme to preserve both mass and energy was illustrated numerically throughout the long-time simulation. This preservation ability reflects the reliability and accuracy of the proposed scheme. The reflections of the soliton waves when colliding the boundaries have been simulated for two types of boundary conditions. The type of the boundary condition affects the wave shape only during the interaction with the wall. In the case of elastic interactions, the vector soliton can do an infinite number of interactions without any change in their shapes except at the boundaries. But for the inelastic scenarios, the soliton wave suffers from a deformation in its shape and some energy decaying, where the daughter waves, small wavelets and radiations begin to appear. The

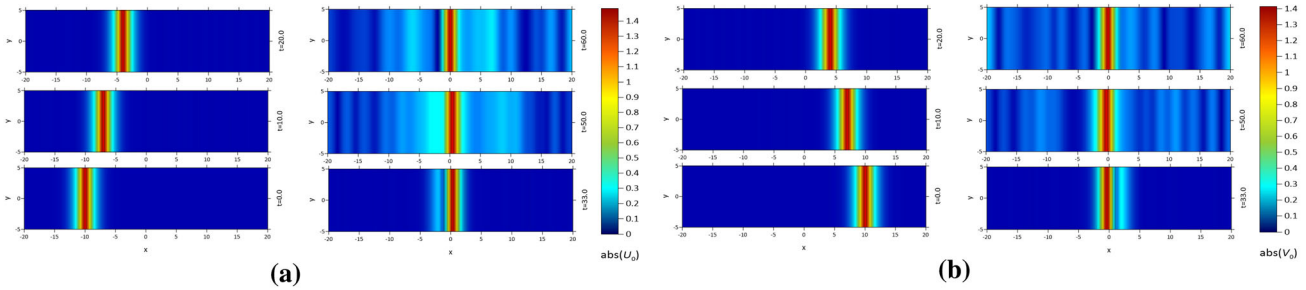

Fig. 13 Trajectory of scenario 5 interactions when $\beta = 0.2$ and $s_1 = -s_2 = 0.3$, (**a**) $|U|$ and (**b**) $|V|$

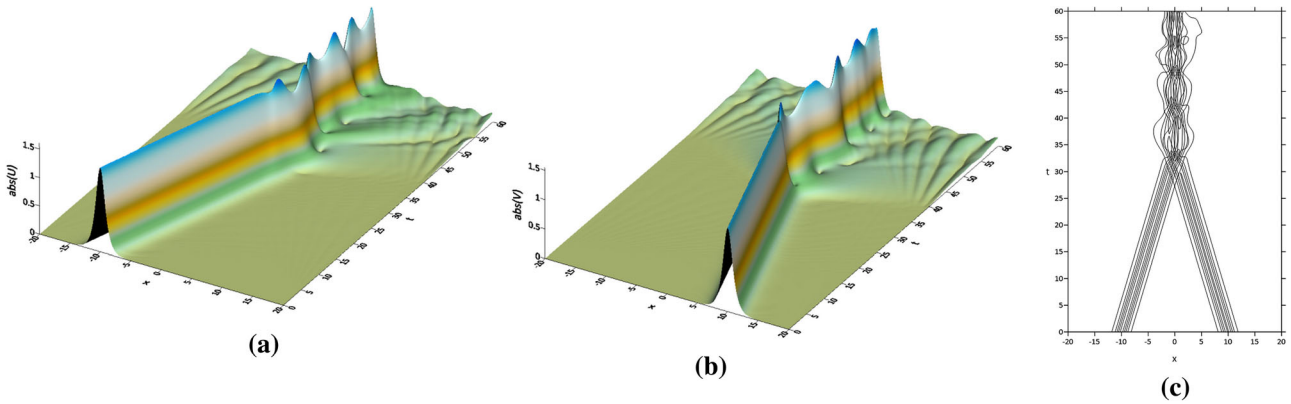

Fig. 14 (**a**) 3D surface plot of $|U|$, (**b**) 3D surface plot of $|V|$ and (**c**) contours plot of $|U|$ and $|V|$ together along the line $y = 0$ when $\beta = 0.2$ and $s_1 = -s_2 = 0.3$

value and sign of the parameter β play an important role in shaping the vector soliton; and in the number of transmitted daughter waves; and in the amount of generated radiations. The speed of initial solitons has a significant impact as well. This work offers new results associated with the interaction and reflection of soliton waves in $(2 + 1)$-dimensional NLS systems. The obtained results are quite general and can be applied to other nonlinear Schrödinger-type systems.

Acknowledgements The first author would like to thank the Deanship of Scientific Research at Majmaah University for supporting this work under Project Number: R-2021-31.

References

[1] A Hasegawa and F Tappert *Appl. Phys. Lett.* **23** 142 (1973).
[2] G P Agrawal *Nonlinear Fiber Optics*. (Berlin: Springer) (2007)
[3] M Wadati and T Iizuka and M Hisakado *J. Phys. Soc. Jpn.* **61** 2241 (1992).
[4] B Guo *Numerical Study of Nonlinear Waves*. (Berlin: Springer) (1995)
[5] J H V Nguyen, P Dyke, D Luo, B A Malomed and R G Hulet *Nat. Phys.* **10** 918 (2014).
[6] Z R Huang, B Tian, Y P Wang and Y Sun *Comput. Math. Appl.* **69** 1383 (2015).
[7] M M Mousa and S F Ragab *Z Naturforsch. Sect. A J. Phys. Sci.* **63** 140 (2008).
[8] J Yang and D J Benney *Stud. Appl. Math.* **96** 111 (1996).
[9] W X Ma *Appl. Math. Lett.* **102** 106161 (2020).
[10] J Yang *Phys. Rev. E Stat. Phys. Plasmas, Fluids, Relat. Interdiscip. Top* **59** 2393 (1999).
[11] A R Osborne, M Onorato and M Serio *Phys. Lett. Sect. A Gen. At. Solid State Phys.* **275** 386 (2000).
[12] M S Ismail *Math. Comput. Simul.* **78** 532 (2008).
[13] S Ertug and A Aydin *Appl. Math. Comput. Sci.* **8** 43 (2016).
[14] A Aydin *Chaos, Solitons Fractals* **41** 735 (2009).
[15] M S Ismail, H A Ashi and F Al-Rakhemy *AIP Conf Proc.* **1648** 1 (2015).
[16] J J Su and Y T Gao *Waves Random Complex Media* **28** 708 (2018).
[17] L L Zhang and X M Wang *Mod. Phys. Lett. B* **34** 1 (2020).
[18] G Biondini and G Hwang *J. Phys. A Math. Theor.* **42** 1 (2009).
[19] G Biondini and A Bui *Stud. Appl. Math.* **129** 249 (2012).
[20] V Caudrelier and Q C Zhang *J. Phys. A Math. Theor.* **45** 1 (2012).
[21] M Wang, W R Shan, X Lü, Y S Xue, Z Q Lin and B Tian *Appl. Math. Comput.* **219** 11258 (2013).
[22] J Q Sun, X Y Gu and Z Q Ma *Phys. D Nonlinear Phenom.* **196** 311 (2004).
[23] M S Ismail and T R Taha *Math. Comput. Simul.* **74** 302 (2007).
[24] Z Fei, V M Pérez-García and L Vázquez *Appl Math. Comput.* **71** 165 (1995).
[25] L R T Gardner, G A Gardner, S I Zaki and Z El Sahrawi *Comput. Methods Appl. Mech. Eng.* **108** 303 (1993).
[26] T Katsaounis and D Mitsotakis *Math. Methods Appl. Sci.* **41** 1013 (2018).
[27] W E Schiesser *The Numerical Method of Lines: Integration of Partial Differential Equations*. (Cambridge: Academic Press) (1991)

[28] M M Mousa and M Reda *Appl. Phys. Res.* **5** 43 (2013).
[29] M M Mousa *Zeitschrift Für Naturforsch A A J. Phys. Sci.* **70** 47 (2015).
[30] M M Mousa *J. Ocean Eng. Sci.* **3** 303 (2018).
[31] M M Mousa and W X Ma *Mod. Phys. Lett. B* **34** 2050051 (2020).
[32] E Isaacson and H B Keller *Analysis of Numerical Methods*. (New York, USA: Dover) (2012)